Optimal depth of subvolcanic magma chamber growth controlled by volatiles and crust rheology

Christian Huber[1], Meredith Townsend[1,2], Wim Degruyter[3], Olivier Bachmann[4]

[1]Department of Earth, Environmental and Planetary Sciences, Brown University, 324 Brook Street, Providence, Rhode Island 02912, USA

[2] Department of Earth Sciences, University of Oregon, 100 Cascade Hall, Eugene, OR 97403, USA

[3]School of Earth and Ocean Sciences, Cardiff University, Main Building, Park Place, Cardiff, CF10 3AT, United Kingdom.

[4]Department of Earth Sciences, ETH Zürich, Clausiusstrasse 25, 8092 Zurich, Switzerland

Storage pressures of magma reservoirs influence the style, frequency and magnitude of volcanic eruptions. Neutral buoyancy or rheological transitions are commonly assumed to control where magmas accumulate and form such reservoirs. However, the density of volatile-rich silicic magmas is typically lower than the surrounding crust, and the rheology of the crust alone does not control the depth of the brittle-ductile transition around a magma reservoir. Yet, typical storage pressures inferred from geophysical inversions or petrological methods seem to cluster around 2 $\pm$ 0.5 kbar in all tectonic settings and crustal compositions. Here, we use thermo-mechanical modeling to show that storage pressure is controlled by volatile exsolution and crustal rheology. At pressures $\lesssim$1.5 kbar, and for geologically realistic water contents, reservoir volumes, and recharge rates, the presence of an exsolved magmatic volatile phase hinders reservoir growth because eruptive volumes are typically larger than recharges feeding the system during periods of dormancy. At pressures $\gtrsim$2.5 kbar, the viscosity of the crust in long-lived magmatic provinces is sufficiently low to inhibit most eruptions. Sustainable eruptible magma reservoirs are able to develop only within a relatively narrow range of pressures around 2 $\pm$ 0.5 kbar, where the amount of exsolved volatiles fosters growth while the high viscosity of the crust promotes the necessary overpressurization for eruption.

Over the last decades, a polybaric view of magmatic differentiation has emerged (see early ideas in [1,2]), referred to as “crustal distillation columns” with multiple levels of storage and differentiation[3]. However, the depth/pressure at which magmas stall and the processes that control those storage depths remain controversial[4]. Magmas are typically thought to accumulate first at the crust-mantle boundary, forming deep crustal mush zones (MASH [5] or hot zones [6]) and then again at shallow depths, potentially leading to two main storage levels[3].

However, other conceptual models have suggested several additional storage levels in the lower to mid-crust ([4,7]).

Magma storage pressure is a fundamental variable that controls volatile exsolution and mineral phase assemblages, impacting chemical differentiation and eruptive styles of magmas as they ascend to the surface. Pressure is unfortunately one of the most difficult thermodynamic variables to constrain; its estimate by any method (e.g., mineral barometry, volatile saturation pressures in melts, geophysical imaging of active systems) is subject to assumptions that can be challenging to validate. Here we present a complementary approach, focusing on mechanical processes thought to play a role in trapping magmas in the crust.

Crustal magma reservoirs are thought to form by the amalgamation of sill- and dike-like intrusions that transport magma vertically from deeper sources ([8-10]). Therefore, understanding the depth at which these reservoirs form requires knowledge about 1) the processes that cause dikes and sills to stall in the subsurface; and 2) the processes that allow subsequent growth of the incipient magma reservoirs[11]. Dike arrest and deflection into sills are largely governed by fracture mechanics, and some commonly cited controls include neutral buoyancy ([12,13]), rheological and rigidity contrasts ([14,15]), and reorientation of stresses ([9]). Although dike propagation occurs over short timescales where the host crust behaves elastically, the growth of subvolcanic magma reservoirs occurs on longer timescales allowing for ductile deformation of the crust to play a role. The observation that magma transport in the upper crust occurs by brittle deformation, while storage requires some amount of crustal creep, is the reason that the "brittle-ductile" transition commonly is invoked as the primary control on the depth of silicic magma reservoirs (e.g.[16-18]).

Brittle-ductile transition and the depth of magma chambers

Within the context of the brittle-ductile transition, a magma chamber can grow if the crust can deform in a ductile manner in response to recharges, limiting the pressure build-up within the magma reservoir and inhibiting eruptions. Although the brittle-ductile transition may influence the depth of emplacement of magma reservoirs, it is an incomplete argument. Indeed, the rheology of the crust – whether it is brittle or ductile – depends not only on the temperature (e.g., [19]) but also on the strain rate. In the context of magma reservoir growth, the strain rate is a function of the rate of pressure build-up in the magma chamber, which depends on the reservoir volume, compressibility, and magma recharge rate[11]. Therefore, even considering the same crustal composition and temperature, the "brittle-ductile transition" may occur at different depths for different rates of pressure loading in the reservoir[20]. Moreover, the conditions required for magma reservoir growth in ***erupting*** systems (mass loss at the surface) remain puzzling. Hence, we focus here on conditions that need to be fulfilled for magma reservoirs to grow while the system remains volcanically active.

We posit here that exsolved magmatic volatiles play an important role in the growth of subvolcanic reservoirs by regulating the size of eruptions. Reservoir growth occurs by recharge (mass addition), and is limited or balanced out by eruption (mass loss). The role of exsolved volatiles is key for eruption volume (e.g., [21]); the presence of an exsolved gas phase in the reservoir can significantly enhance the mass of magma erupted during a single event. Additionally, 3-phase thermo-mechanical modeling of volcanic systems demonstrated that exsolved volatiles damp the build-up of pressure in shallow magma reservoirs caused by recharges during periods between eruptions[22,23]. The presence and exsolution of volatiles therefore exerts a fundamental control on the proportion of the magma emplaced in the reservoir that is later erupted, and hence the propensity of magma reservoirs to grow, stall or shrink over time[24,21].

A multiphase framework for magma reservoir evolution is required to identify the conditions that are most favorable to the growth of large eruptible chambers of silicic magmas in the crust. We consider the magma chamber to be the eruptible portion of the magma reservoir, which contains the chamber as well as the surrounding mush. The physical model used here includes (1) a visco-elastic rheology for the host response to pressure changes in the chamber and (2) the evolution of an open multiphase magma chamber (crystal-melt-exsolved volatiles) in response to magma recharges, eruptions, and cooling[25]. The model, based on mass and enthalpy conservation equations (see Supplementary material), was run for more than 500 simulations initiated at a temperature of 930 °C just below the magma liquidus (950 °C) and stopped when the magma reached a critical crystallinity of 50 vol. %, where it is assumed no longer eruptible. These >500 simulations cover a parameter space of initial magma water content that ranges from 4 to 7 wt% (increments of 1 wt%), lithostatic pressure from 1 to 3 kbar (increments of 0.25 kbar), initial eruptible volumes in the chamber ranging from 0.1 to 10 km^3 and long-term averaged magma recharge rates of 10^{-5} to 10^{-3} km^3/yr. We consider a continuous and fixed set of recharge rates because our objective is to understand the growth and eruptible behavior of chambers over their lifespan rather than single events of recharge and their eruption triggering potential. The effect of short-term transient variations in recharge rate on magma chamber dynamics was studied in ref. [22].

The background geotherm (in the far-field) is set to 30 °C/km, such that the far-field temperature varies with the storage depth (a range of far-field geotherms is considered in the supplementary material). The temperature-dependent flow law for the rheology of the crust (from [26]) is the same as the one previously used in thermo-mechanical models[27,28]. The goal of the simulations is to determine the subdomain in parameter space (initial chamber volume, recharge rate, depth and magma water content) where the following two conditions are satisfied: (1) the magma chamber grows (by mass) over the course of the simulation and (2) the magma chamber is capable of eruptions (mass withdrawal from the chamber). As such, we are not considering internal processes such as mixing or chemical zonation or stratification, but focus on the balance between pressure evolution, crustal response, and crystallization-exsolution that is essential to capture the long-term evolution (growth and eruption) of these magma bodies.

Grow versus blow

The processes that govern repose and eruption cycles at volcanoes are complex and tightly coupled. It is possible, however, to characterize the dynamics of a chamber subjected to magma injection and eruptions using a simplified framework that consists of three competing timescales[25]:

- The cooling timescale of a magma body is defined by $\tau_{cool}=R^2/\kappa$ with R a characteristic length-scale of the chamber (or effective radius), κ the thermal diffusivity of host rocks. This timescale controls the internal evolution of the magma chamber in terms of volume fraction of melt, crystals and exsolved volatiles. By extension, it affects the thermal and mechanical response of the magma body to recharges and eruptions.
- The relaxation timescale $\tau_{relax} = \eta_{eff}/\Delta p_c$, where η_{eff} is the effective flow law of the crustal material evaluated at initial conditions (here taken from [26]) and Δp_c

is the critical overpressure that leads to eruptions. The relaxation timescale characterizes the ability of the crust to relax changes in pressure in the chamber by creep.

- The injection timescale $\tau_{inj}=M/\dot{M}_{inj}$, with $\dot{M}_{inj}$ the mass influx rate of magma into the chamber and M the mass of magma already present in the chamber. By convention, we report the injection rate in units of $km^3/yr = \dot{M}_{inj}/\rho$, where ρ is the density of the magma injected.

From these three timescales, we define two dimensionless ratios $\theta_1=\tau_{cool}/\tau_{inj}$ (akin to a Peclet number) and $\theta_2= \tau_{relax}/\tau_{inj}$ (akin to a Deborah number).

On the basis of several hundreds of simulations run at a fixed pressure of 2 kbar and considering a magma containing initially 5 wt% water (Figure 1), three different regimes can be identified:

1. the chamber grows and erupts over the course of the simulation; this occurs when the injection timescale is smaller than both relaxation and cooling timescales ($\theta_1>1$ and $\theta_2>1$),
2. the chamber grows but does not erupt, leading to the growth of plutonic roots. This regime occurs when the relaxation timescale is short compared to the injection timescale (crust is compliant and efficient at dissipating overpressure), and $\theta_2/\theta_1<1$,
3. the chamber erupts but shrinks (more mass is erupted than added by recharges over time; $\theta_2>1$ and $\theta_1<1$), leading to shrinking chambers.

The boundaries between these domains illustrate that both internal (cooling causing crystallization and exsolution, pressure increase by recharges) and external factors (rheology of the crust) control magma chamber growth, stability and longevity.

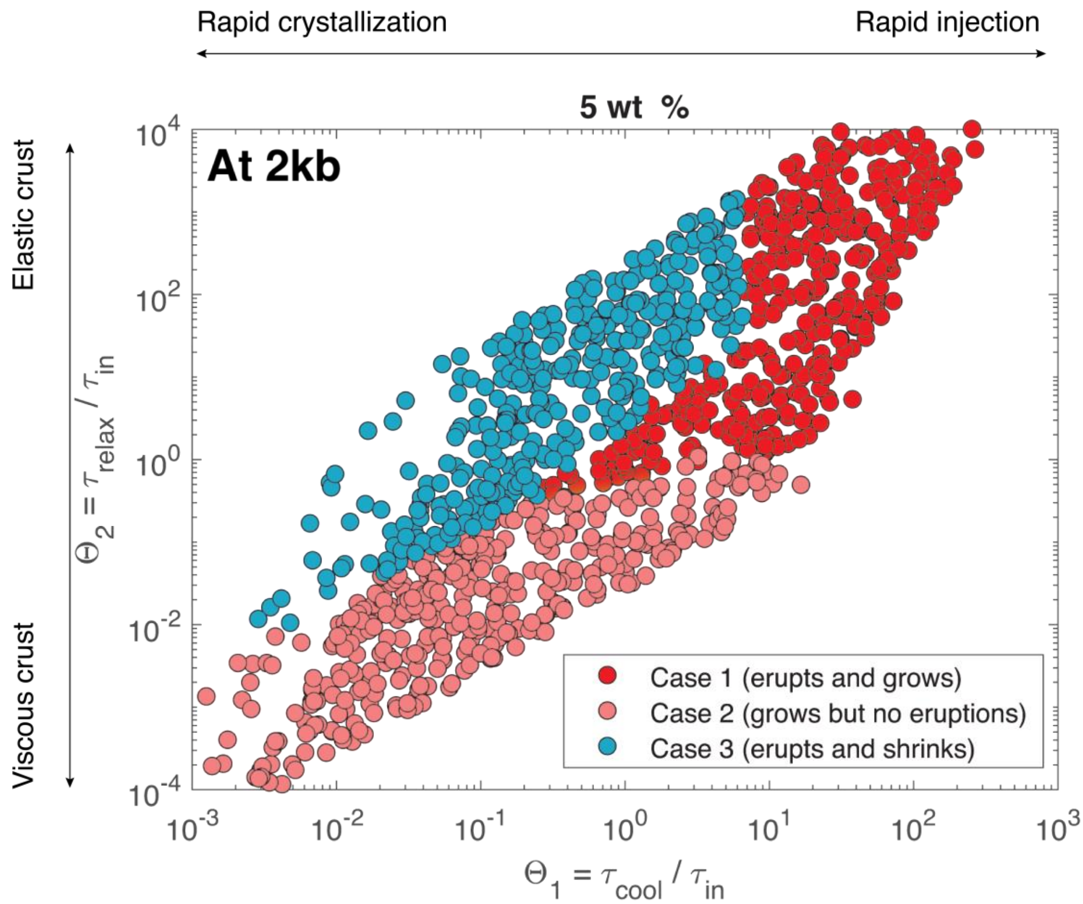

*Figure 1: **Regime diagram showing the evolution of magma chambers at a pressure of 2 kbar**. The magma contains initially 5 wt % water. The x-axis refers to the ratio of the cooling and injection timescales (more rapid injection rates to the right) and the y-axis describes the ability of the crust to accommodate the mass change in the chamber (high = elastic behavior of the crust, low ductile deformation). Additional simulations tested with a different critical overpressure (20 MPa) show a qualitatively similar behavior with a slightly larger domain for simulations that undergo eruptions (case 1).*

A sweet spot around 2 kbar

Running additional simulations over a range of depth (i.e. lithostatic pressure and temperature) and magma water content values leads to three major observations (Figure 2). First, some conditions of magma recharge and initial magma chamber size do not yield any solution for chambers simultaneously growing and erupting. This is true for large chambers and small recharge fluxes and it is consistent with recharges being too weak to trigger eruptions[25]. Second, the pressure range where magma chambers are found to grow while being tapped by eruptions (in red) is restricted around 2 $\pm$ 0.5 kbar. Third, the boundary between eruptible and non-eruptible growing magma chambers (Case 1 and 2) is dominantly vertical to subvertical (i.e., independent of the water content in the chamber), implying that the transition is largely independent of the internal state of the chamber; it is mostly controlled by the depth of the chamber, the size of the chamber and the magma recharge rate. As the recharge rate increases, the boundary shifts to greater depth because pressure-build-up is more rapid and can compete with the timescale for host-rock to relax stress by creep at greater depths. Considering fast recharge rates, an opposite effect (shallowing of the boundary) occurs with increasing chamber volume, because, for a given recharge rate, pressure build-up is slower in a larger chamber and therefore more prone to be accommodated by creep in the host rocks.

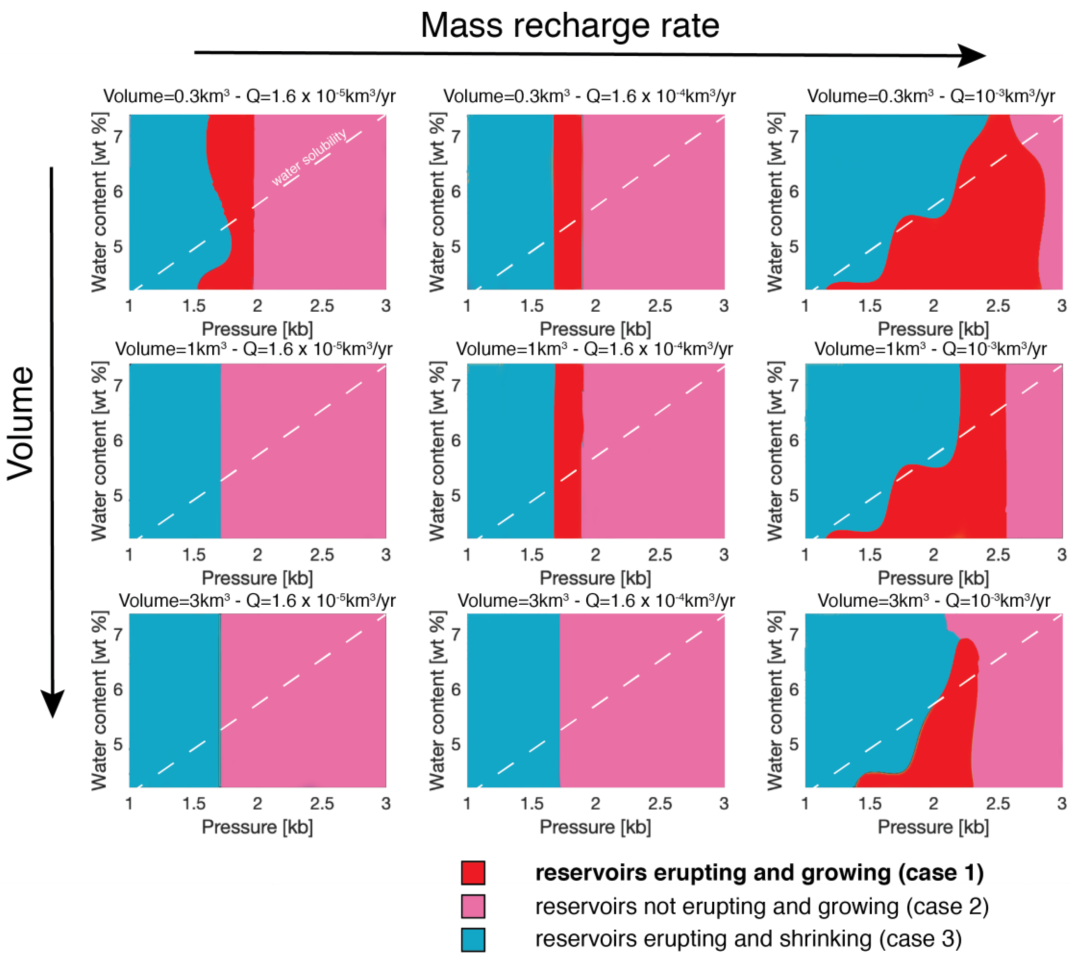

Figure 2. ***Regime diagrams of eruptible and growing chambers as function of magma water content, depth, magma recharge rate and initial volume****. Each plot shows three regions. The blue region represents conditions that are favorable to volcanic eruptions, but where the mass of magma stored shrinks with time (short-lived systems that cannot build up to large volumes). The red region highlights the regime where magma chambers are eruptible and grow. The pink region shows the regime where magma chambers grow, but do not erupt (will ultimately form plutonic material). The white dashed line shows the water solubility curve (based on [29]).*

The boundary that separates the two regimes of eruptible chambers (case 1 and 3) at low pressure is also dominantly sub-vertical. At high water content (> 5 wt% H_2O), saturation in a Magmatic Volatile Phase (MVP) is reached at or near the liquidus while at slightly lower water content (~4 wt %), MVP saturation is reached after only a few tens of percent crystallization. This behavior is consistent with the shallowing of the transition between growing and shrinking chambers to follow a trend subparallel to the slope of the solubility curve (white dashed line) for chambers subjected to fast recharge rates and magmas with low water content.

The cause for overall mass loss in shallow chambers (<~1.5 kbar) is cooling and crystallization-driven exsolution during the interval between eruptions (dormancy periods). If a chamber can significantly exsolve volatiles during its repose phase, the eruption volume and mass can exceed the mass supplied by recharges (this is true for all recharge rates tested here). This also explains the shallowing of the transition at low water content, because the behavior is mostly absent in chambers that do not undergo significant second boiling. In addition, the cooling caused by an eruption is more significant for chambers containing a significant mass of exsolved volatiles. The smaller erupting chambers will therefore also cool faster, creating a positive feedback that leads to rapid solidification.

Pressure at storage conditions

A large proportion of petrological studies rely on melt inclusion data or mineral barometry (see compilation by [4,30-33]). However, trapping melt inclusions typically occurs during rapid mineral growth, potentially leading to boundary layer effects[34] and behavior as imperfect pressure vessels, especially in mineral phases that cleave or crack easily (such as plagioclases or pyroxenes). During decompression associated with eruptions, melt inclusions can leak and record low pressures that may not relate to the reservoir conditions (e.g., recording depths of < 2-3 km, [35-37]). For silicic magmas, studies that report compositions of pristine quartz-hosted melt inclusions likely provide the most reliable pressure estimates (e.g., [38-40]). Similarly, mineral barometry suffers from inaccuracies related to the fact that compositional parameters in minerals are not only pressure-sensitive, but also strongly depend on temperature and melt composition. For example, when amphibole phenocrysts grow from a melt that is saturated with multiple other phases (e.g., quartz, biotite, 2 feldspars), then the degrees of freedom in the melt composition are limited (system is said to be compositionally buffered), and pressure values tend to be more reliable using the latest barometric calculations (see for example [41,42]). However, when magmas have less mineral diversity, amphibole compositions can strongly vary as a function of melt composition, and barometric calculations can be unreliable[43,31].

Constraining the volume and depth of shallow magma reservoirs from geophysical images is also challenging because resolution is typically low, and active volcanoes often host a hydrothermal system above the reservoir, where hot fluids circulate in the permeable crust [18]. From geophysical inversions, hydrothermal systems are not easy to distinguish from regions where silicate melt accumulates, because both share similar signatures (density significantly lower than surrounding crust, high electric conductivity, low Vs, high Vp/Vs, e.g., [44-46]). Similarly, during unrest periods at a volcanic edifice, it is expected that the hydrothermal circulation and possibly boiling of water can lead to pressure changes that are detected by geodetic surveys[47,48], leading again to a bias for shallow structures.

With these caveats in mind, we summarize published petrologic and geophysical data on storage depths for various volcanic centers (Figure 3). While this is not an exhaustive list, the data selected follows selection criteria discussed above (e.g., quartz-hosted melt inclusions, pristine amphibole composition with buffering mineral assemblage, well-characterized experimental constraints). All three independent techniques (mineral and melt inclusion barometry and geophysical imaging) converge towards an average pressure 2 ± 0.5 kbar for the emplacement of the subvolcanic reservoirs that feed most intermediate to silicic eruptions. This optimal pressure range is well known to experimental petrologists, who commonly use 2 kbar as the default pressure for many of their runs[49-51]. This observation holds true across tectonic settings, and all differentiation trends.

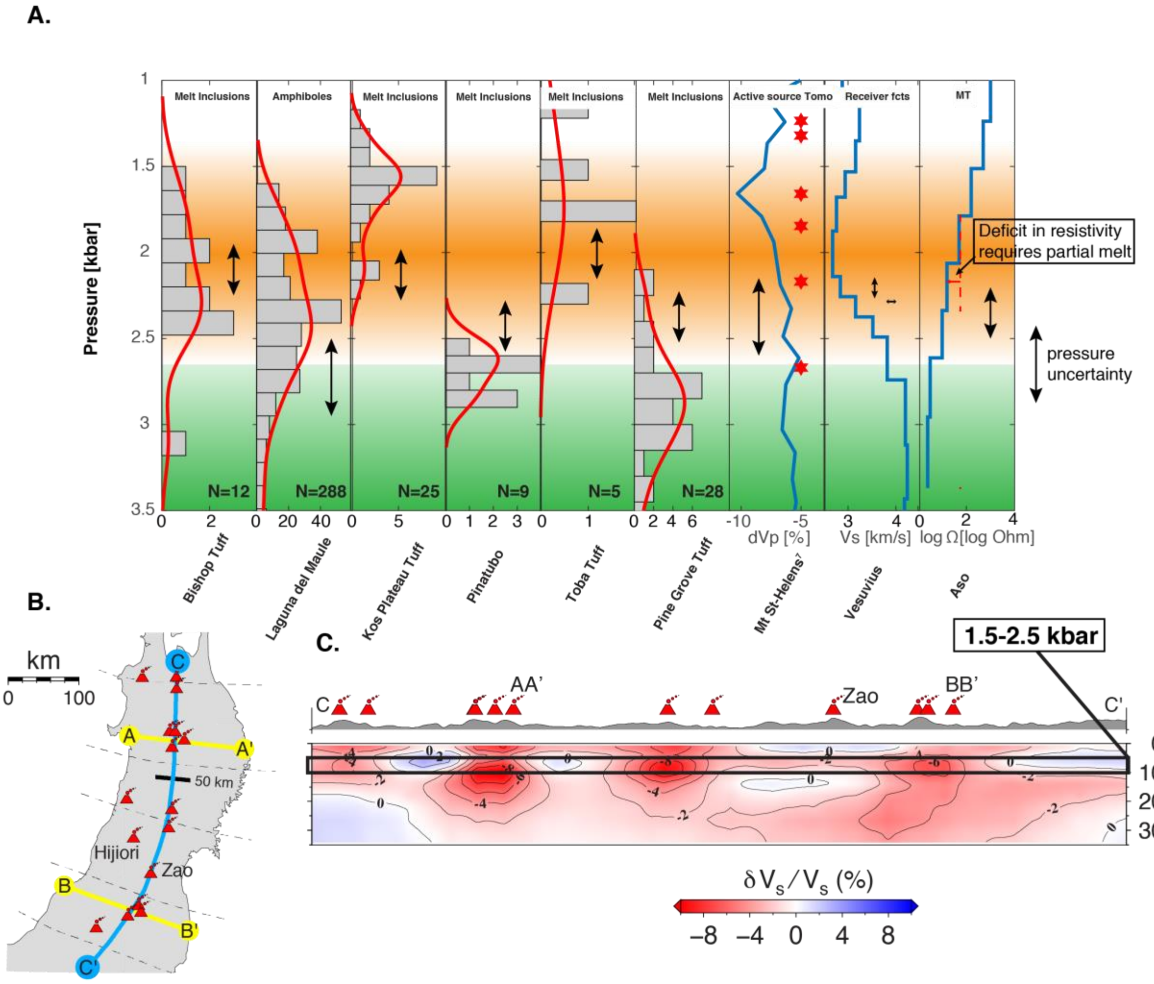

*Figure 3. **Pressure distribution where melt/active magma reservoir is inferred from petrology or geophysical methods**. In A, double arrows represent pressure uncertainty as provided by the referenced studies; Bishop Tuff[40], Kos Plateau Tuff[38], Pinatubo[52], Toba Tuff[53] and Pine Grove[54] estimates from melt inclusions (in quartz), Laguna del Maule[55] from amphibole geobarometry. St Helens, Vesuvius and Aso pressure distributions are retrieved from geophysical inversion on Vp[56], Vs[57], and Magnetotellurics[58]. Stars for St Helens refer to pressure estimates from experimental petrology[59,50]. Depth to pressure conversion assumes here a crust with an average density of 2750 kg/m^3. B and C: map and Vs profile in Northern Japan (modified from[60]).*

Evolution and imaging of magmatic columns

Our model results provide a process-based understanding on several important aspects of polybaric evolution in water-rich silicic magma reservoirs in the middle to upper crust. These reservoirs are able to form around pressures of about 1.5-2.5 kbar because (1) the crust is compliant enough to host growing magma bodies and (2) the abundance of exsolved volatiles and efficiency of exsolution is limited enough for eruptions not to mobilize more magma than what is supplied. Interestingly, although magma reservoirs are able to grow more efficiently at pressures above 2.5 kbar in our model, the magma emplaced at these depths or deeper does generally not contribute directly to the volcanic record unless exceptionally large recharge rates are considered (long-term averaged fluxes >>10^{-3} km^3/yr).

Our simulations suggest that (1) only transient magma bodies (unable to grow to any significant size) form at pressures below 1.5 kbar, (2) eruptible and long-lived (potentially large) bodies form between 1.5 and 2.5 kbar and (3) large non-eruptible feeding/recharge roots emplace below, in excellent agreement with experimental petrology[61,62], observations from geophysical imaging[63,64,56,65,66], melt inclusion data[38,40] and mineral and melt barometry[55,67] for different silicic volcanic centers that are capable of eruption volumes spanning 3 orders of magnitude (Figure 4). With variable tectonic stresses, as well as magma and volatile compositions, the pressure bounds (here suggested to be ~1.5 to 2.5 kbar) will change slightly, but the existence of an optimal entrapment depth in the upper crust for erupting reservoirs will abide.

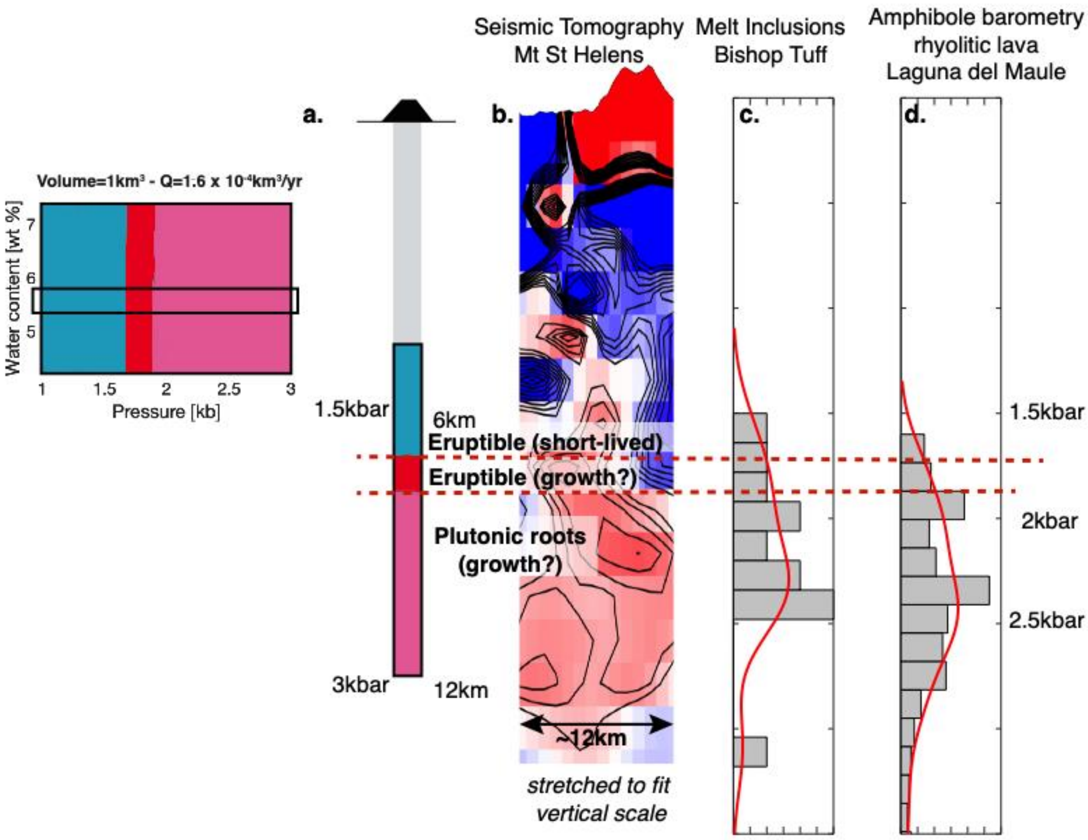

Figure 4. Summary diagram comparing numerical simulations with geophysical and petrological data. Example from a numerical simulation of Figure 2 and comparison with seismic tomography (active) at Mt St-Helens[56], melt inclusion data from the Bishop Tuff, Long Valley caldera[40] and amphibole geobarometry at Laguna del Maule, Chile[55].

Data and code availability

This project did not produce new data. Codes and simulations outputs are available upon request to christian_huber@brown.edu.

Acknowledgements

The authors would like to thank Kai-Xun Chen for providing panels B and C of figure 3 under a format that allowed us to modify the figure. C.H. is funded through an NSF CAREER grant, M. T. is funded through NSF-EAR 1760004 awarded to C.H., and O. B. by the Swiss National Fund 200021_178928. The authors thank four anonymous reviewers for comments that significantly improved the manuscript.

References

1 Hildreth, W. Gradients in silicic magma chambers: Implications for lithospheric magmatism. *Journal of geophysical research* **86**, 10153-10192 (1981).

2 Lipman, P. W., Doe, B. & Hedge, C. Petrologic evolution of the San Juan volcanic field, Southwestern Colorado: Pb and Sr isotope evidence. *Geological Society of America Bulletin* **89**, 59-82 (1978).

3 Bachmann, O. & Huber, C. Silicic magma reservoirs in the Earth's crust. *American Mineralogist* **101**, 2377-2404 (2016).

4 Cashman, K. V., Sparks, R. S. J. & Blundy, J. D. Vertically extensive and unstable magmatic systems: A unified view of igneous processes. *Science* **355** (2017).

5 Hildreth, W. S. & Moorbath, S. Crustal contributions to arc magmatism in the Andes of Central Chile. *Contributions to Mineralogy and Petrology* **98**, 455-499 (1988).

6 Annen, C., Blundy, J. D. & Sparks, R. S. J. The genesis of intermediate and silicic magmas in deep crustal hot zones. *Journal of Petrology* **47**, 505-539 (2006).

7 Marsh, B. D. A magmatic mush column Rosetta Stone: the McMurdo Dry Valleys of Antarctica. *EOS Transactions, American Geophysical Union* **85**, 497-502 (2004).

8 Burchardt, S. New insights into the mechanics of sill emplacement provided by field observations of the Njardvik Sill, Northeast Iceland. *Journal of Volcanology and Geothermal Research* **173**, 280-288, doi:https://doi.org/10.1016/j.jvolgeores.2008.02.009 (2008).

9 Menand, T. Physical controls and depth of emplacement of igneous bodies: A review. *Tectonophysics* **500**, 11-19, doi:https://doi.org/10.1016/j.tecto.2009.10.016 (2011).

10 Miller, C. F. *et al.* Growth of plutons by incremental emplacement of sheets in crystal-rich host: Evidence from Miocene intrusions of the Colorado River region, Nevada, USA. *Tectonophysics* **500**, 65-77 (2011).

11 Karlstrom, L., Paterson, S. R. & Jellinek, A. M. A reverse energy cascade for crustal magma transport. *Nature Geoscience* **10**, 604, doi:10.1038/ngeo2982 https://www.nature.com/articles/ngeo2982#supplementary-information (2017).

12 Lister, J. R. & Kerr, R. C. Fluid-mechanical models of crack propagation and their application to magma transport in dykes. *Journal of Geophysical Research: Solid Earth* **96**, 10049-10077, doi:10.1029/91JB00600 (1991).

13 Walker, G. P. L. Gravitational (density) controls on volcanism, magma chambers and intrusions. *Australian Journal of Earth Sciences* **36**, 149-165 (1989).

14 Gudmundsson, A. Magma chambers: Formation, local stresses, excess pressures, and compartments. *Journal of Volcanology and Geothermal Research* **237,Äì238**, 19-41, doi:10.1016/j.jvolgeores.2012.05.015 (2012).

15 Rivalta, E., Taisne, B., Bunger, A. P. & Katz, R. F. A review of mechanical models of dike propagation: Schools of thought, results and future directions. *Tectonophysics* **638**, 1-42, doi:http://dx.doi.org/10.1016/j.tecto.2014.10.003 (2015).

16 Burov, E., Jaupart, C. & Guillou-Frottier, L. Ascent and emplacement of buoyant magma bodies in brittle-ductile upper crust. *Journal of Geophysical Research* **108, NO. B4, 2177** (2003).

17 Gregg, P. M., de Silva, S. L., Grosfils, E. B. & Parmigiani, J. P. Catastrophic caldera-forming eruptions: Thermomechanics and implications for eruption triggering and maximum caldera dimensions on Earth. *Journal of Volcanology and Geothermal Research* **241-242**, 1-12, doi:http://dx.doi.org/10.1016/j.jvolgeores.2012.06.009 (2012).

18 Lowenstern, J. B., Smith, R. B. & Hill, D. P. Monitoring super-volcanoes: geophysical and geochemical signals at Yellowstone and other large caldera systems. *Phil. Trans. R. Soc. A* **364**, 2055–2072 (2006).

19 Gettings, M. E. Variation of depth to the brittle-ductile transition due to cooling of a midcrustal intrusion. *Geophysical research Letters* **15**, 213-216 (1988).

20 Rubin, A. M. Dike ascent in partially molten rock. *Journal of Geophysical Research: Solid Earth* **103**, 20901-20919, doi:10.1029/98JB01349 (1998).

21 Huppert, H. E. & Woods, A. W. The role of volatiles in magma chamber dynamics. *Nature* **420**, 493-495 (2002).

22 Degruyter, W., Huber, C., Bachmann, O., Cooper, K. M. & Kent, A. J. R. Magma reservoir response to transient recharge events: The case of Santorini volcano (Greece). *Geology* **44**, 23-26, doi:10.1130/G37333.1 (2016).

23 Degruyter, W., Huber, C., Bachmann, O., Cooper, K. M. & Kent, A. J. R. Influence of Exsolved Volatiles on Reheating Silicic Magmas by Recharge and Consequences for Eruptive Style at Volcán Quizapu (Chile). *Geochemistry, Geophysics, Geosystems* **18**, 4123-4135, doi:10.1002/2017GC007219 (2017).

24 Forni, F., Degruyter, W., Bachmann, O., De Astis, G. & Mollo, S. Long-term magmatic evolution reveals the beginning of a new caldera cycle at Campi Flegrei. *Science Advances* **4** (2018).

25 Degruyter, W. & Huber, C. A model for eruption frequency of upper crustal silicic magma chambers. *Earth and Planetary Science Letters* **403**, 117-130, doi:http://dx.doi.org/10.1016/j.epsl.2014.06.047 (2014).

26 Hansen, F. D. & Carter, N. L. in *The 24th U.S. Symposium on Rock Mechanics (USRMS)* 20 (American Rock Mechanics Association, College Station, Texas, 1983).

27 Jellinek, A. M. & DePaolo, D. J. A model for the origin of large silicic magma chambers: precursors of caldera-forming eruptions. *Bulletin of Volcanology* **65**, 363-381 (2003).

28 Karlstrom, L., Dufek, J. & Manga, M. Magma chamber stability in arc and continental crust. *Journal of Volcanology and Geothermal Research* **190**, 249-270 (2010).

29 Liu, Y., Zhang, Y. & Behrens, H. Solubility of H2O in rhyolitic melts at low pressures and a new empirical model for mixed H2O-CO2 solubility in rhyolitic melts. *Journal of Volcanology and Geothermal Research* **143**, 219-235 (2005).

30 Johnson, M. C. & Rutherford, M. J. Experimental calibration of the aluminum-in-hornblende geobarometer with application to Long Valley Caldera (California) volcanic rocks. *Geology* **17**, 837-841 (1989).

31 Putirka, K. Amphibole thermometers and barometers for igneous systems and some implications for eruption mechanisms of felsic magmas at arc volcanoes. *American Mineralogist* **101**, 841 (2016).

32 Schmidt, M. W. Amphibole composition in tonalite as a function of pressure; an experimental calibration of the Al-in-hornblende barometer. *Contributions to Mineralogy and Petrology* **110**, 304-310 (1992).

33 Wallace, P. J., Anderson, A. T. & Davis, A. M. Quantification of pre-eruptive exsolved gas contents in silicic magmas. *Nature* **377**, 612-615 (1995).

34 Baker, D. R. The fidelity of melt inclusions as records of melt composition. *Contributions to Mineralogy and Petrology* **156**, 377-395, doi:10.1007/s00410-008-0291-3 (2008).

35 Blundy, J. D. & Cashman, K. V. Rapid decompression-driven crystallization recorded by melt inclusions from Mount St. Helens volcano. *Geology* **33**, 793–796 (2005).

36 Lloyd, A. S., Plank, T., Ruprecht, P., Hauri, E. H. & Rose, W. Volatile loss from melt inclusions in pyroclasts of differing sizes. *Contributions to Mineralogy and Petrology* **165**, 129-153, doi:10.1007/s00410-012-0800-2 (2013).

37 Wallace, P. in *Melt Inclusions in Volcanic Systems: Methods, Applications and Problems* Vol. 5 (eds B. De Vivo & R.J. Bodnar) 105-127 (Elsevier Science, Developments in Volcanology, 2003).

38 Bachmann, O., Wallace, P. J. & Bourquin, J. The melt inclusion record from the rhyolitic Kos Plateau Tuff (Aegean Arc). *Contributions to Mineralogy and Petrology* **159**, 187-202, doi:Doi 10.1007/S00410-009-0423-4 (2010).

39 Lowenstern, J. B. in *Melt Inclusions in Volcanic Systems: Methods, Applications and Problems.* Vol. Developments in Volcanology 5 (eds B. De Vivo & R.J. Bodnar) 1-22 (Elsevier Press, 2003).

40 Wallace, P. J., Anderson, A. T. & Davis, A. M. Gradients in H_2O, CO_2, and exsolved gas in a large-volume silicic magma chamber: interpreting the record preserved in the melt inclusions from the Bishop Tuff. *Journal of Geophysical Research* **104**, 20097-20122 (1999).

41 Ague, J. J. Thermodynamic calculation of emplacement pressures for batholithic rocks, California; implications for the aluminum-in-hornblende barometer. *Geology* **25**, 563-566 (1997).

42 Bachmann, O. & Dungan, M. A. Temperature-induced Al-zoning in hornblendes of the Fish Canyon magma, Colorado. *American MIneralogist* **87**, 1062-1076 (2002).

43 Erdmann, S., Martel, C., Pichavant, M. & Kushnir, A. Amphibole as an archivist of magmatic crystallization conditions: problems, potential, and implications for inferring magma storage prior to the paroxysmal 2010 eruption of Mount Merapi, Indonesia. *Contributions to Mineralogy and Petrology* **167**, 1-23, doi:10.1007/s00410-014-1016-4 (2014).

44 Bedrosian, P. A., Peacock, J. R., Bowles-Martinez, E., Schultz, A. & Hill, G. J. Crustal inheritance and a top-down control on arc magmatism at Mount St Helens. *Nature Geoscience* **11**, 865-870, doi:10.1038/s41561-018-0217-2 (2018).

45 Hata, M., Takakura, S., Matsushima, N., Hashimoto, T. & Utsugi, M. Crustal magma pathway beneath Aso caldera inferred from three-dimensional electrical resistivity structure. *Geophysical Research Letters* **43**, 10,720-710,727, doi:10.1002/2016GL070315 (2016).

46 Miller, C. A., Le Mével, H., Currenti, G., Williams-Jones, G. & Tikoff, B. Microgravity changes at the Laguna del Maule volcanic field: Magma-induced stress changes facilitate mass addition. *Journal of Geophysical Research: Solid Earth* **122**, 3179-3196, doi:doi:10.1002/2017JB014048 (2017).

47 Chaussard, E. & Amelung, F. Regional controls on magma ascent and storage in volcanic arcs. *Geochemistry, Geophysics, Geosystems* **15**, 1407-1418, doi:doi:10.1002/2013GC005216 (2014).

48 Hurwitz, S., Kipp, K. L., Ingebritsen, S. E. & Reid, M. E. Groundwater flow, heat transport, and water table position within volcanic edifices: Implications for volcanic processes in the Cascade Range. *Journal of Geophysical Research-Solid Earth* **108** (2003).

49 Holtz, F., Sato, H., Lewis, J. F., Behrens, H. & Nakada, S. Experimental Petrology of the 1991-1995 Unzen Dacite, Japan. Part I: Phase Relations, Phase Composition and Pre-eruptive Conditions. *Journal of Petrology* **46**, 319-337, doi:10.1093/petrology/egh077 (2005).

50 Rutherford, M. J., Sigurdsson, H., Carey, S. & Davis, A. M. The May 18, 1980, eruption of Mount St. Helens, 1. Melt composition and experimental phase equilibria. *Journal of Geophysical Research* **90**, 2929-2947 (1985).

51 Scaillet, B., Holtz, F. & Pichavant, M. Experimental Constraints on the Formation of Silicic Magmas. *Elements* **12**, 109-114, doi:10.2113/gselements.12.2.109 (2016).

52 Wallace, P. J. & Gerlach, T. M. Magmatic Vapor Source For Sulfur-Dioxide Released During Volcanic-Eruptions - Evidence From Mount-Pinatubo. *Science* **265**, 497-499 (1994).

53 Chesner, C. A. & Luhr, J. F. A melt inclusion study of the Toba Tuffs, Sumatra, Indonesia. *Journal of Volcanology and Geothermal Research* **197**, 259-278, doi:https://doi.org/10.1016/j.jvolgeores.2010.06.001 (2010).

54 Lowenstern, J. B., Bacon, C. R., Calk, L. C., Hervig, R. L. & Aines, R. D. Major-element, trace-element, and volatile concentrations in silicate melt inclusions from the tuff of Pine Grove, Wah Wah Mountains, Utah. 20 (U.S. Geological Survey Open-File Report 94-242, 1994).

55 Andersen, N. L. *et al.* Pleistocene to Holocene Growth of a Large Upper Crustal Rhyolitic Magma Reservoir beneath the Active Laguna del Maule Volcanic Field, Central Chile. *Journal of Petrology* **58**, 85-114, doi:10.1093/petrology/egx006 (2017).

56 Kiser, E., Levander, A., Zelt, C., Schmandt, B. & Hansen, S. M. Focusing of melt near the top of the Mount St. Helens (USA) magma reservoir and its relationship to major volcanic eruptions. *Geology*, doi:10.1130/G45140.1 (2018).

57 Agostinetti, N. P. & Chiarabba, C. Seismic structure beneath Mt Vesuvius from receiver function analysis and local earthquakes tomography: Evidences for location and geometry of the magma chamber. *Geophysical Journal International* **175**, 1298-1308, doi:10.1111/j.1365-246X.2008.03868.x (2008).

58 Hata, M. *et al.* Three-Dimensional Electrical Resistivity Distribution Beneath the Beppu–Shimabara Graben With a Focus on Aso Caldera, Southwest Japan Subduction Zone. *Journal of Geophysical Research: Solid Earth* **123**, 6397-6410, doi:10.1029/2018JB015506 (2018).

59 Gardner, J. E., Carey, S., Rutherford, M. J. & Sigurdsson, H. Petrologic Diversity in Mount St-Helens Dacites During the Last 4,000 Years - Implications for Magma Mixing. *Contributions to Mineralogy and Petrology* **119**, 224-238 (1995).

60 Chen, K.-X., Gung, Y., Kuo, B.-Y. & Huang, T.-Y. Crustal Magmatism and Deformation Fabrics in Northeast Japan Revealed by Ambient Noise Tomography. *Journal of Geophysical Research: Solid Earth* **123**, 8891-8906, doi:doi:10.1029/2017JB015209 (2018).

61 Johnson, M. & Rutherford, M. Experimentally determined conditions in the Fish Canyon Tuff, Colorado, magma chamber. *Journal of Petrology* **30**, 711-737 (1989).

62 Scaillet, B. & Evans, B. W. The 15 June 1991 eruption of Mount Pinatubo. I. Phase equilibria and pre-eruption P-T-fO_2-fH_2O conditions of the dacite magma. *Journal of Petrology* **40**, 381-411 (1999).

63 Huang, H.-H. *et al.* The Yellowstone magmatic system from the mantle plume to the upper crust. *Science* **348**, 773-776, doi:10.1126/science.aaa5648 (2015).

64 Huang, Y.-C., Ohkura, T., Kagiyama, T., Yoshikawa, S. & Inoue, H. Shallow volcanic reservoirs and pathways beneath Aso caldera revealed using ambient seismic noise tomography. *Earth, Planets and Space* **70**, 169, doi:10.1186/s40623-018-0941-2 (2018).

65 Masturyono, McCaffrey, R., Wark, D. A. & Roecker, S. W. Distribution of magma beneath the Toba caldera complex, north Sumatra, Indonesia, constrained by three-dimensional P wave velocities, seismicity, and gravity data. *Geochemistry, Geophysics, Geosystems* **2** (2001).

66 Fedi, M. *et al.* Gravity modeling finds a large magma body in the deep crust below the Gulf of Naples, Italy. *Scientific Reports* **8**, 8229, doi:10.1038/s41598-018-26346-z (2018).

67 Gualda, G. A. R. & Ghiorso, M. S. Low-pressure origin of high-silica rhyolites and granites. *The Journal of Geology* **121**, 537-545, doi:10.1086/671395 (2013).

Methods

The physical model is based on the conservation of total mass, water and enthalpy in a homogeneous magma chamber (see reference [25]), and it is discussed in greater details in the extended methods. The overpressure threshold set for the initiation of dikes was 20 MPa, but similar results were obtained with 40 MPa. The datasets generated during this study (outputs from numerical simulations) and the codes used to generate the results are available from the corresponding author.

1. Model Description

We use the physical model of Degruyter and Huber (2014) and extended by Townsend et al. (2019) to describe the evolution of a magma reservoir. The model is designed to study the interaction of first-order processes that govern the capability for a magma reservoir to grow and erupt during its lifetime. The model considers an eruptible portion of magma referred to as the magma chamber sitting in a colder, viscoelastic region that represents the transition from a mush in the proximity of the chamber to the surrounding crust in the far field. We assume that the main processes involved are (1) magma recharge, (2) crystallization, (3) volatile exsolution, (4) heat loss to the surroundings, (5) viscoelastic response of the surroundings in response to volume changes in the chamber, and (6) mass withdrawal due to eruptions (Figure S1).

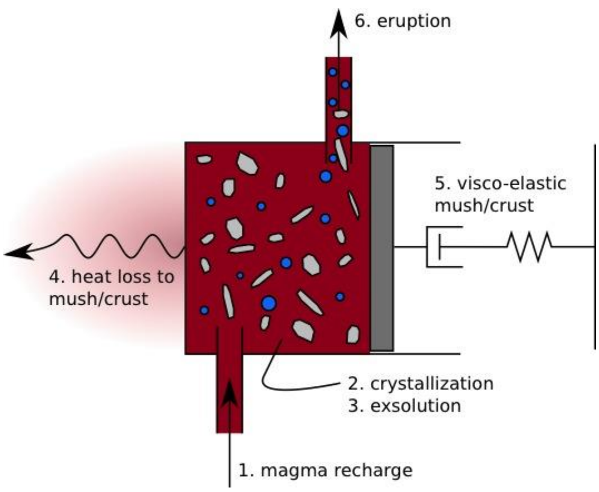

Figure S1: Schematic diagram of the model.

1.1 Governing equations

The governing equations of the model are conservation of mass, water, and energy applied to the magma chamber, which we can write concisely as:

$$\frac{dM}{dt} = \dot{M}_{in} - \dot{M}_{out} , \qquad \text{(S1)}$$

$$\frac{dM^w}{dt} = \dot{M}^w_{in} - \dot{M}^w_{out} , \qquad \text{(S2)}$$

$$\frac{dH}{dt} = \dot{H}_{in} - \dot{H}_{out} , \qquad \text{(S3)}$$

where M, M^w, and H represent the (total) mass, the water mass and the enthalpy of the magma chamber, respectively. The subscripts "*in*" and "*out*" indicate source and sink terms, respectively.

1.2 Constitutive equations

The time evolution of the magma chamber volume (V), melt (ρ_m) and crystal density (ρ_X) are described by the following relationships:

$$\frac{dV}{dt} = \frac{1}{\beta_r}\frac{dP}{dt} + \frac{\Delta P}{\eta_r} - \alpha_r \frac{dT}{dt}, \qquad \text{(S4)}$$

$$\frac{d\rho_m}{dt} = \frac{1}{\beta_m}\frac{dP}{dt} - \alpha_m \frac{dT}{dt}, \qquad \text{(S5)}$$

$$\frac{d\rho_X}{dt} = \frac{1}{\beta_X}\frac{dP}{dt} - \alpha_X \frac{dT}{dt}, \qquad \text{(S6)}$$

with T temperature and P pressure in the chamber. α and β are the thermal expansion coefficient (10^{-5} K^{-1}) and bulk modulus (10^{10} Pa), respectively. The subscripts *m*, *X, and r* refer to the melt phase, crystal phase, and the mush/country rocks, respectively. ΔP indicates the overpressure, i.e. the chamber pressure minus the lithostatic pressure. η_r is the effective viscosity of the surrounding shell.

The crystallization in the chamber is described by a parameterized relationship between the temperature and the crystal volume fraction defined by equation (13) in Huber *et al.* (2009). We use an exponent of b=0.5, 700°C for the solidus and 950°C for the liquidus temperature, which are values representative for silicic magmas. We assume water is the dominant volatile species. We use the solubility model of Zhang (1999) as parameterized in equation (16) of Dufek and Bergantz (2005), suitable for water in rhyolite. To determine the density of the exsolved volatile phase we use the modified Redlich-Kwong relationship of Halbach and Chatterjee (1982) as parameterized in equation (7) of Huber *et al.* (2010).

1.3 Boundary conditions

We assume that magma is supplied continuously from deeper levels in the crust at a constant rate, which we vary between 10^{-5} and 10^{-3} km^3/yr in agreement with long-term rates suggested for volcanic systems (White *et al.*, 2006). The temperature of the injected magma is assumed to be the 927°C (1200K) and its water content is equal to the initial water content of the chamber.

Mass withdrawal due to eruptions occurs when overpressure in the magma chamber reaches a critical overpressure of 20 MPa (40 MPa was also tested and lead to similar results). The value of a critical overpressure is uncertain and has been suggested to fall anywhere between 1 and 100 MPa (Grosfils 2007; Gudmundsson, 2012, Grosfils et al., 2015). The values we use here are based on scaling arguments based on the cooling of a dike (Jellinek & DePaolo, 2003, Rubin, 1995). We also require that the magma remains mobile for an eruption to occur. The physical properties of the magma removed from the chamber are set equal to those within the chamber. We simply set this criterion equivalent to having less than or equal to 0.5 crystal volume fraction, a value commonly used (Marsh, 1981). Once this crystal volume fraction is reached through sufficient cooling, the calculation is stopped.

The heat loss from the chamber to the surroundings is determined at each time step from an analytical solution whereby the chamber is considered a hot sphere sitting in a larger sphere with a radius ten times the radius of the initial chamber. The initial temperature profile between the inner and outer sphere is assumed to be at steady state and thus assumes a mature plumbing system. The temperature at the inner boundary is that of the magma chamber and that at the outer boundary is set at a constant value in accordance with the crustal temperature in the far field at the depth of the magma chamber. To obtain this temperature we assume a geothermal gradient of 30°C/km for all the calculation in the main paper. In the next section we examine the influence of a hotter geotherm (40°C/km), as well as varying this temperature independently from the assumed depth of the chamber. The temperature profile evolves over time in response to changes in temperature of the magma chamber taking into account the history of the temperature changes (see appendix A.4 in Degruyter and Huber (2014)). From this profile the heat flow rate emanating from the chamber is calculated.

The temperature profile of the shell is also used to determine η_r, the effective viscosity of the surrounding shell. At each position z in the shell a viscosity $\eta(z)$ is determined using an Arrhenius law

$$\eta(z) = Ae^{\left(\frac{G}{BT(z)}\right)} \qquad \text{(S7)}$$

with A=4.27x10^7 Pa s a material dependent constant, G= 141x10^3 J/mol the activation energy for creep flow, B=8.31 J/mol/K the molar gas constant, $T(z)$ the temperature at that position in the shell. We base equation (S7) on the discussion of (Jellinek & DePaolo, 2003) that uses values for Westerly granite with 0.1 wt water based on experiments from Hansen and Carter (1983) . The effective viscosity of the shell is calculated from averaging across the radially varying viscosity within the shell following the method of Lensky *et al.* (2001). See appendix A.5 in Degruyter and Huber (2014) for further details.

1.4 Initial conditions

Together with recharge rate, three initial conditions are varied to explore parameters space. The initial pressure is set equal to the lithostatic pressure. Assuming a crustal density of 2750 kg/m^3 and a storage depth between 6 and 12 km, we evaluate storage depth between 1 and 3 kbar. The choice of depth also determines the temperature of the outer shell of the surroundings, which is calculated using the geothermal gradient as discussed in the previous section. The initial volume of the chamber ranges between 0.1 and 10 km^3 and the initial magma water content ranges from 4 to 7 wt%. The initial temperature and density of the melt and crystal phase are the same for all calculations and are 927°C (1200 K), 2400 kg/m^3, and 2600 kg/m^3, respectively.

2. The effect of different crustal geotherms

We ran additional simulations with a hotter far-field geotherm to test how it influences the most favorable depth of emplacement of a magma reservoir over various conditions (depth, water content in the magma, initial volume and recharge rate). It is important to note however that the near-field temperature field around the chamber (here near-field refers to a distance shorter than 10 times the chamber radius) is initially set to be at steady-state with the hot magma reservoir (thermally mature crust) and is solved analytically accounting for the temperature variation in the chamber at any subsequent time. The far-field geotherm is therefore influencing the boundary condition in the far-field only. As expected, the results obtained with a hotter geotherm 40°C/km are very similar to the results we obtained with 30°C/km. The main difference is that the maximum depth for an eruptible magma reservoir is shallower (lower pressure) for the higher geotherm simulations, as expected.

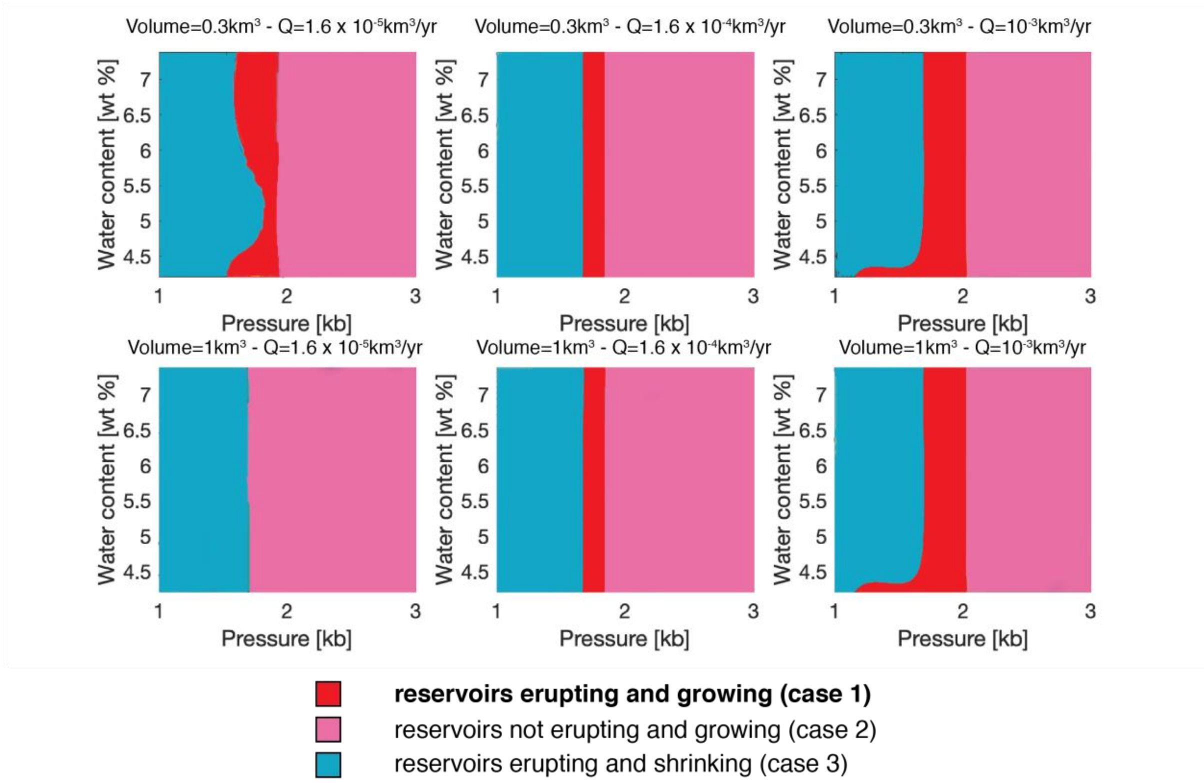

Figure S2. Example of simulations of magma chamber evolution under a higher far-field geotherm (40 °C/km). The main conclusions from the lower T far-field geotherm still hold true, the boundary between regime 1 and 2 is shifted to lower pressure (shallower depth) as expected from a warmer crust, albeit by < 0.5 kbar for the larger chambers (even less for smaller chambers).

We conducted a series of magma chamber simulations to establish whether the sweet spot observed in Figure 2 and S2 (in pressure or depth range, where magma chambers can both grow and erupt), is robust when considering a wide range of pressure-temperature (P-T) crustal conditions (Figs. S3 and S4 show results for an initial magma water content of 4 and 6 wt.%, respectively). The temperature on the x-axis in these figures corresponds to the temperature assumed at the outer boundary of the surrounding shell as explained in section 1.3 above. This is equivalent to the "unperturbed" crustal temperature at the same depth as the centroid of the magma chamber in the far-field. Some of the most extreme P-T conditions explored are not realistic and we bracketed the most likely conditions between two endmember geotherms of 30 and 50°C/km. In all cases, we observe that magma chambers shrink in mass at the lowest pressure (in general a depth corresponding to pressures below 1.5 kbar) while growth (by mass) is promoted at higher pressure. We also find that eruptions are suppressed when considering far-field crustal temperature at an equivalent depth that go beyond a critical temperature that ranges between 250 and 375°C and equivalent pressure ranging from 2 to 3 kbar in our simulations. The variation in critical temperature and pressure marking the transition from an eruptible to a non-eruptible chamber is mostly driven by the size and recharge rate of the chamber, which again supports the importance of conditions such as the volume of the chamber and recharge rate of magma on the brittle-ductile transition.

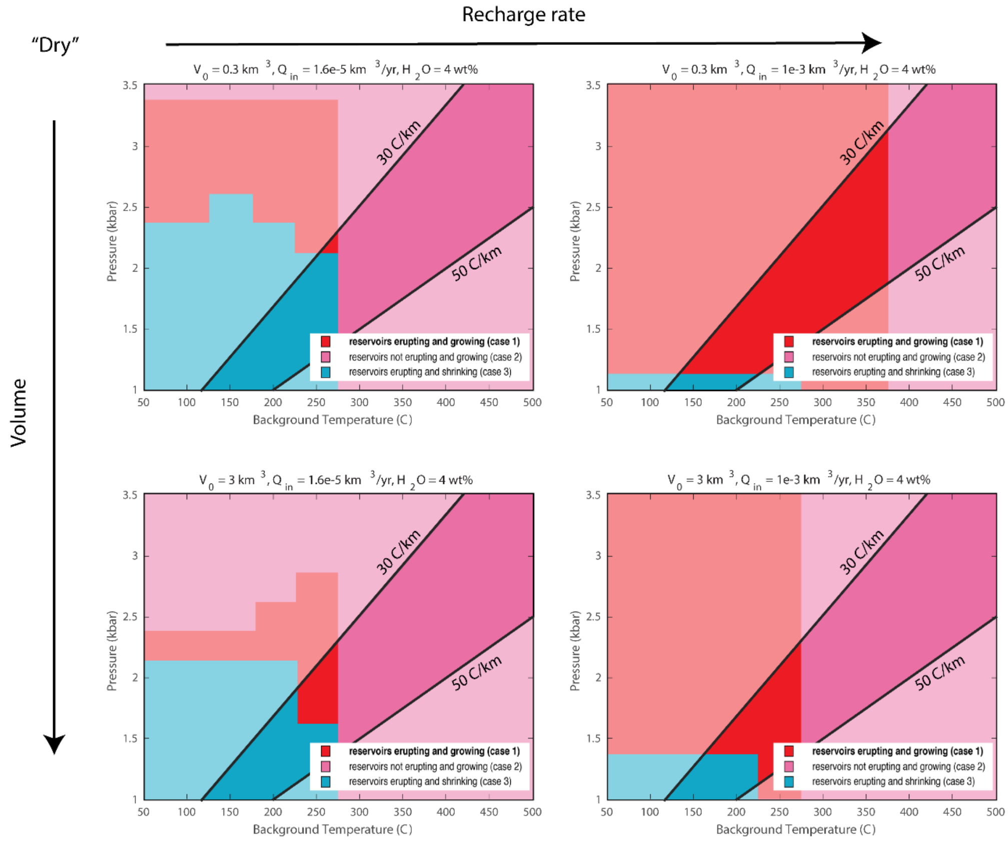

Figure S3. P-T regime diagrams showing the regimes of growth and eruption of subvolcanic magma chambers in a dryer scenario (magma with initially 4 wt % water). We selected two endmember geothermal gradients which bracket the most reasonable range of P-T conditions for magma chamber evolution.

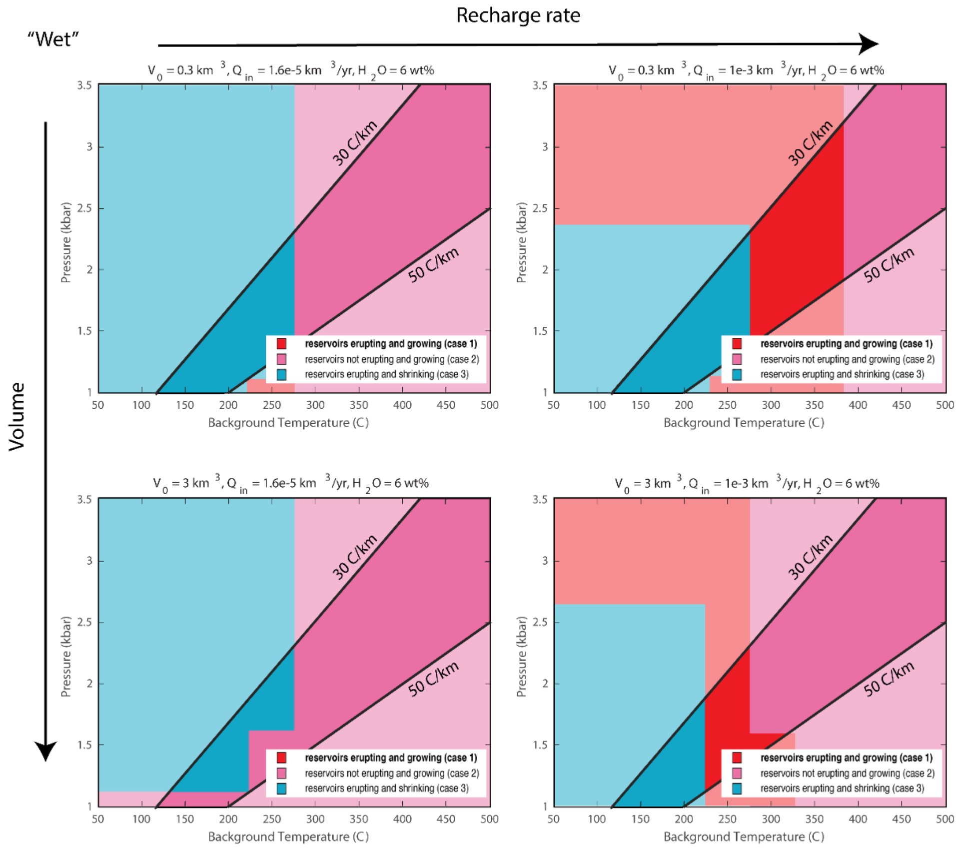

Figure S4. Similar diagram as Figure S3, but considering a wet magma with initially 6 wt % water.

References

Degruyter, W. & Huber, C. (2014). A model for eruption frequency of upper crustal silicic magma chambers. *Earth and Planetary Science Letters* **403**, 117-130.

Dufek, J. & Bergantz, G. W. (2005). Transient two-dimensional dynamics in the upper conduit of a rhyolitic eruption: a comparison of closure models for the granular stress. *Journal of Volcanology and Geothermal Research* **143**, 113-132.

Grosfils, E.B., (2007). Magma reservoir failure on the terrestrial planets: Assessing the importance of gravitational loading in simple elastic models, *Journal of Volcanology and Geothermal Research*, Volume **166**, Issue 2, Pages 47-75.

Grosfils, E.B., McGovern, P.J., Gregg, P.M., Galgana, G.A., Hurwitz, D.M., Long, S.M., and Chestler, S.R., (2015). Elastic models of magma reservoir mechanics: a key tool for investigating planetary volcanism, *Geological Society*, London, Special Publications, **401**, 239-267.

Gudmundsson, A. (2012). Magma chambers: Formation, local stresses, excess pressures, and compartments. *Journal of Volcanology and Geothermal Research* **237,Äì238**, 19-41.

Halbach, H. & Chatterjee, N. D. (1982). An empirical Redlich-Kwong Equation of State for Water to 1000 ºC and 200 kbar. *Contributions to Mineralogy and Petrology* **79**, 337-345.

Hansen FD, Carter NL (1983) Semibrittle creep of dry and wet Westerly granite at 1,000 MPa. 24th US Symposium on Rock Mechanics, Texas A&M, pp 429–447.

Huber, C., Bachmann, O., Manga, M. (2009). Homogenization processes in silicic magma chambers by stirring and mushification (latent heat buffering). *Earth and Planetary Science Letters* **283**, 38-47.

Huber, C., Bachmann, O., Manga, M. (2010). Two Competing Effects of Volatiles on Heat Transfer in Crystal-rich Magmas: Thermal Insulation vs Defrosting. *Journal of Petrology* **51**, 847-867.

Jellinek, A. M. & DePaolo, D. J. (2003). A model for the origin of large silicic magma chambers: precursors of caldera-forming eruptions. *Bulletin of Volcanology* **65**, 363-381.

Lensky, N. G., Lyakhovsky, V., Navon, O. (2001). Radial variations of melt viscosity around growing bubbles and gas overpressure in vesiculating magmas. *Earth and Planetary Science Letters* **186**, 1-6.

Marsh, B. D. (1981). On the crystallinity, probability of occurrence, and rheology of lava and magma. *Contributions to Mineralogy and Petrology* **78**, 85-98.

Rubin, A. M. (1995). Propagation of Magma-Filled Cracks. *Annual Review of Earth and Planetary Sciences* **23**, 287-336.

Townsend, M., Huber, C., Degruyter, W., and Bachmann, O. (2019), Magma chamber growth during inter-caldera periods: insights from thermo-mechanical modeling with applications to Laguna del Maule, Campi Flegrei, Santorini, and Aso, *Geochemistry, Geophysics, Geosystems.*

White, S. M., Crisp, J. A., Spera, F. A. (2006). Long-term volumetric eruption rates and magma budgets. *Geochem. Geophys. Geosyst.* **7**.

Zhang, Y. (1999). H2O in rhyolitic glasses and melts: Measurement, speciation, solubility, and diffusion. *Reviews of Geophysics* **37**, 493-516.